Biosensors and Bioelectronics 67 (2015) 621–624

Contents lists available at ScienceDirect

Biosensors and Bioelectronics

journal homepage: www.elsevier.com/locate/bios

A biomimetic sensor for the detection of lead in water

Wendy Chu [a], Yuanchao Zhang [a,b], Da Li [a], Colin J. Barrow [a], Hongbin Wang [c], Wenrong Yang [a,c,*]

[a] School of Life and Environmental Sciences, Deakin University, Vic. 3217, Australia
[b] College of Chemistry and Chemical Engineering, Ocean University of China, Qingdao 266100, China
[c] School of Chemistry and Biotechnology, Yunnan Minzu University, Kunming 650031, China

ARTICLE INFO

Article history:
Received 6 June 2014
Received in revised form
5 September 2014
Accepted 27 September 2014
Available online 2 October 2014

Keywords:
Gold nanoparticle
Core–satellite
Self-assembly
Lead
Glutathione
Colorimetric

ABSTRACT

The monitoring of lead (II) ions (Pb^{2+}) in water is essential for both human health and the environment. Herein, a simple yet innovative biosensor for Pb^{2+} detection is presented. The sensor is developed by the self-assembly of gold nanoparticles (GNPs) core–satellite structure using naturally occurring tripeptide glutathione (GSH) as linker. The addition of Pb^{2+} caused a red-to-blue color change and the localized surface plasmon resonance (LSPR) band was shifted to *ca.* 650 nm. The limit of detection (LOD) is found to be 47.6 nM (9.9 ppb) by UV–vis spectroscopy with high selectivity against other heavy metals. This method offers a new strategy for heavy metal detection using functionalized GNPs.

1. Introduction

Lead (Pb^{2+}) is a toxic heavy metal which commonly contaminates water. Tiny amount of Pb^{2+} will eventually accumulate into fatal level due to its non-biodegradable nature. It damages many organ systems, including the central nervous system, reproductive system, liver and kidney. Children are more susceptible to the effects of Pb^{2+}, and there are evidences suggesting exposure to low level of Pb^{2+} is associated with attention deficit hyperactivity disorder (ADHD), lower IQ and higher risk of childhood aggression (Jakubowski, 2011; Kim et al., 2013; Liu, 2011). Therefore, the monitoring of Pb^{2+} in water is essential for both human health and the environment.

Many methods have been developed to detect Pb^{2+}, for example, inductively coupled plasma mass spectroscopy was used to detect Pb^{2+} in parts per trillion level (Stetzenbach et al., 1994). Although spectroscopic techniques like ICP-AES or ICP-MS can detect Pb^{2+} with high sensitivity, they require large and cumbersome instruments. While previous electrochemical approaches had high-sensitivity, but lacked selectivity for specific ions. (Chai et al., 2010; Cho et al., 2012; Guo et al., 2013). The limited approaches can provide sensitivity below pico-molar to study the accumulation of much diluted metal for public health concern (Cho et al., 2012). Therefore, there is an urgently need to develop a sensitive, simple, fast and cost effective method for Pb^{2+} detection.

Gold nanoparticles (GNPs) have been widely used in sensing applications due to their unique size and shape dependent optical properties. Localized surface plasmon resonance (LSPR), the collective oscillation of surface electrons due to the excitation of incident light, is one of the most important properties of GNPs. The binding of analyte to GNPs causes red-shift in SPR peak can be used for GNPs-based colorimetric sensing (Fu et al., 2012; Huang et al., 2010; Kalluri et al., 2009; Li et al., 2010). The surface modification of GNPs is essential to provide chemical functionality. Careful selection and design of ligands for surface modification of GNPs strongly influence the sensitivity and selectivity of a sensor. It has been shown that core–satellite GNPs structure is able to provide higher sensitivity compared with uniform size GNPs (Choi et al., 2012). For example, DNA has been widely used as a linker in the self-assembly of core–satellite structures (Chen et al., 2010; Chou et al., 2014; Pal et al., 2009; Schreiber et al., 2013; Sebba and Lazarides, 2008; Sebba et al., 2008). We have recently demonstrated the linkage of large and small GNPs coated with L-cysteine as core–satellite by Cu^{2+} (Weng et al., 2013). Coupled plasmonic assembly of colloidal gold and silver has also been reported (Choi et al., 2012; Encina and Coronado, 2010). However, to our

* Corresponding author at: School of Life and Environmental Sciences, Deakin University, Vic 3217, Australia.
E-mail address: wenrong.yang@deakin.edu.au (W. Yang).

http://dx.doi.org/10.1016/j.bios.2014.09.077
0956-5663/

knowledge, no core–satellite structure utilizing peptide as a linker is studied.

Here, a new strategy for Pb^{2+} detection based on the self-assembly of core satellite GNP structure by glutathione (GSH) is demonstrated. GSH is a naturally occurring tripeptide which can be found in both animals and plants. It has strong affinity to the GNPs, due to the thiol group of cysteine residue, which can form self-assembled monolayer on GNPs. It also contains hydrophilic functional groups, including two carboxyl groups and one amine group, which can chelate with metal ions. Moreover, the overall negative charge of GSH molecule provides repulsive force which prevent aggregation of GNPs after ligand exchange reaction. Some studies demonstrated that Pb^{2+} caused changes in the level of GSH in mammalian, fish, spider and plant tissues (Canesi et al., 1999; Wilczek et al., 2004; Yadav, 2010). Thus, it is hypothesized that GSH can chelate with Pb^{2+} and produce detectable signals via GNPs to allow the development of biomimetic sensors for Pb^{2+} detection. In this study, a colorimetric detection method for Pb^{2+} using GSH–GNPs core–satellite structure was developed. The limit of detection (LOD) was found to be 47.6 nM (9.9 ppb) by UV–vis spectroscopy with high selectivity against other heavy metals in standardized solutions.

2. Material and methods

2.1. Materials and apparatus

Gold (III) chloride trihydrate ($HAuCl_4 \cdot 3H_2O$, 99.9+% metals basis), lead (II) nitrate (Pb_2NO_6, ACS reagent, ≥99.0%), L-glutathione reduced ($C_{10}H_{17}N_3O_6S$, ≥98.0%), sodium chloride (NaCl, AR grade, ≥99%), sodium citrate tribasic dihydrate ($C_6H_5Na_3O_7 \cdot 2H_2O$, ACS reagent, ≥99.0%) and different metal salts were purchased from Sigma-Aldrich and used as received. Milli-Q water (18 MΩ cm) was used to prepared all aqueous solutions.

pH of GNPs solutions was measured by Oakton® pH 2700 pH/mV/°C/°F Meter (Oakton Instruments, Illinois,USA). UV–vis spectroscopy was carried out using CARY 300 Bio UV–vis spectrometer (Agilent Technologies, California, USA) with Hellma® Analytics 100-QX Quartz SUPRASIL® 300 Precision cells (light path 1 mm) (Hellma Analytics, Müllheim, Germany). The image of core–satellite structure was visualized using ZEISS Supra 55VP scanning electron microscope (SEM) (ZEISS, Oberkochen, Germany). Surface-enhanced Raman spectroscopy (SERS) was conducted by Renishaw Invia Raman Microspectrometer (Renishaw plc, Gloucestershire, UK) with a 633 nm HeNe laser (RL633 HeNe, Renishaw plc, Gloucestershire, UK) and a thermo-electrical cooled CCD detector using 10 seconds exposure time.

2.2. Colorimetric detection of Pb^{2+}

Approximately 2.5×10^{-4} M GNPs were synthesized as reported previously (Weng et al., 2013). To prepare the Pb^{2+} mediated GNPs core–satellite structure, 13 nm and 45 nm GNPs were mixed in 1:1 ratio (v/v) followed by the addition of GSH which gave the final concentration of peptide at about 100 μM. The solution was incubated for 30 min at room temperature. A series of aliquots of Pb^{2+} solution and 1 M NaCl solution, acting as aggregating agent, were added to 500 μL of GSH–GNPs solution, and incubated for 30 min at room temperature before performing UV–vis spectroscopy. The ratio of absorbance at 650 nm to 525 nm (A_{650}/A_{525}) was used to express the molar ratio of aggregated to disperse GNPs. Three independent readings were taken for each sample and the protocol used for colorimetric detection was illustrated in Fig. 1. To investigate the selectivity of core–satellite structure for Pb^{2+}, other metal ions (Ca^{2+}, Cd^{2+}, Co^{2+}, Cu^{2+}, Fe^{2+}, Mg^{2+}, Mn^{2+} and Ni^{2+}) were studied under the same condition. Lake water collected from Deakin University Waurn Ponds Campus, VIC, Australia was used to confirm the practical application of the assay.

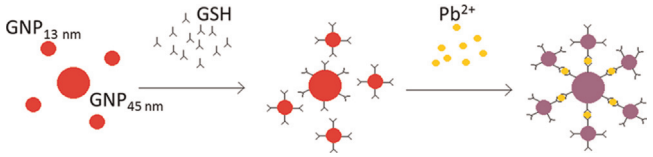

Fig. 1. Schematic representation of the formation of Pb^{2+} mediated core satellite structure.

3. Results and discussion

3.1. Characterization of CORE-satellite structure

The pH of mixture of 13 nm and 45 nm GNPs (1:1 v/v) was around 5.5, which is slightly below the reported pI of GSH (Cutrignelli et al., 2014). The LSPR peak of the mixture was found to be *ca.* 525 nm, which was in between the peak of 13 nm and 45 nm GNPs. The solution remained red in the absence of Pb^{2+}. After addition of Pb^{2+}, the solution turned blue. A newly formed peak was observed at *ca.* 650 nm (Fig. S1), which was caused by the surface plasmon coupling between the satellites and the core. Fig. 2a showed the SEM image of core–satellite structures mediated by Pb^{2+}.

3.2. Optimization of the assay

To optimize experimental condition, the effect of different ratio of 13 nm to 45 nm GNPs, overall concentration of GSH and pH to Pb^{2+} induced self-assemble of core–satellite structures were tested. The self-assemblies of 1:1, 3:1, 4:1, 7:1 and 9:1 (v/v) of 13 nm to 45 nm GSH–GNPs solutions in the presence of Pb^{2+} were recorded by UV–vis spectrometry (Fig. S2). The optimum ratio of 13 nm GNPs to 45 nm GNPs was expected to be equal to the amount of 13 nm GNPs to fully cover the surface of 45 nm GNPs. An approximate particle number ratio of 40:1 ($(45/13)^3$) of 13 to 45 nm GNPs can be deduced for 1:1 (v/v) of 13 to 45 nm GNPs solutions by the diameters of GNPs. Based on UV–vis spectrum, 1:1 (v/v) of 13 nm GNPs to 45 nm GNPs solution showed the best result as the 650 nm peak appeared in the shortest time. The 525 nm peak decreased, and the 650 nm peak increased with time, indicating the formation of aggregated GNPs from dispersed GNPs.

The overall concentrations of GSH of 10, 50, 100 and 150 μM were used to functionalize the 1:1 (v/v) GNPs mixture (Fig. S3). It turn out that 100 μM GSH is best. The experimental results indicated that excess or limited GSH might hinder the formation of Pb^{2+} mediated core–satellite structures.

Then pH were optimized (Fig. S4). At pH 3, the peak at 650 nm appeared before addition of Pb^{2+}, indicating aggregation by GSH–GSH interaction, but not the GSH–Pb^{2+} chelation. Although it has been reported that GSH–GNPs specifically detected Pb^{2+} at pH 8 (Beqa et al., 2011; Chai et al., 2010; Mao et al., 2011), in our system, no aggregation was recorded at this pH. We also found the self-assembly was also not favorable at more basic environment (pH 9). The UV–vis spectrum showed slight increase of 650 nm peak at pH 6, but best result was obtained at pH 5.5. This might be due to curvature effect of various diameters of GNPs. According to the pKa equilibrium of GSH (Fig. S5), in a solution at pH 3.59 to 8.75, majority of GSH would be in the form composing of a protonated amino group and two deprotonated carboxyl groups.

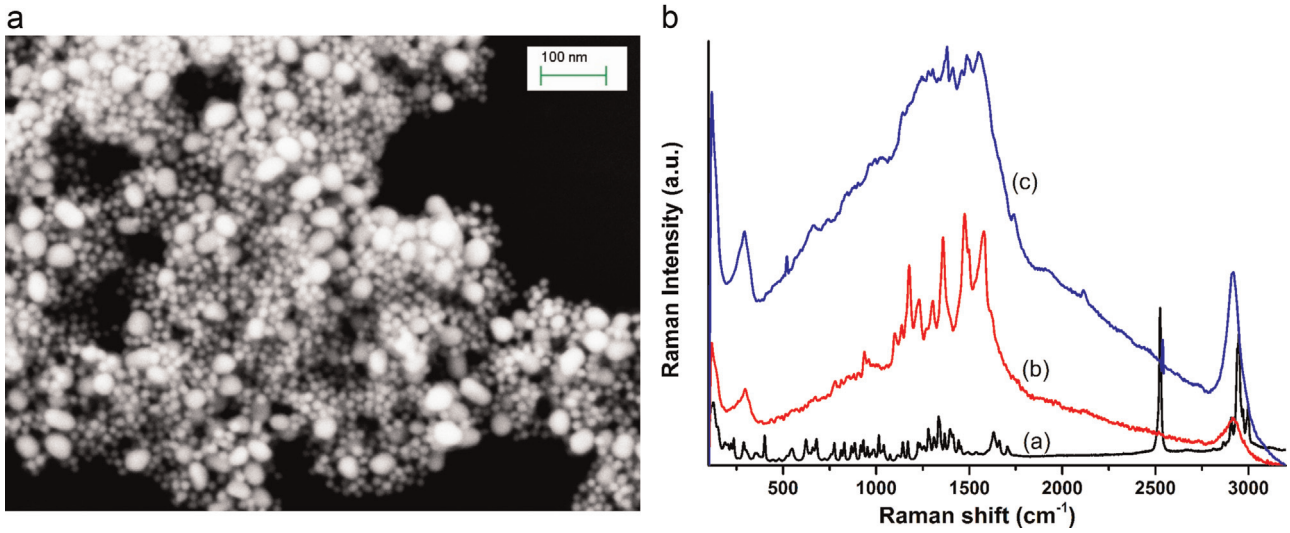

Fig. 2. (a) SEM image of Pb^{2+} mediated core–satellite structure. (b) Raman spectra using 633 nm excitation laser. (a) GSH powder (black); (b) GSH–GNPs before Pb^{2+} addition (red); (c) GSH–GNPs after Pb^{2+} addition (blue). (For interpretation of the references to color in this figure legend, the reader is referred to the web version of this article.)

3.3. SERS spectra of GSH–GNPs before and after Pb^{2+} addition

SERS was conducted to further understand the nature of the self-assembly of Pb^{2+} mediated GSH–GNPs core–satellite structure. Since the LSPR peak shifted to *ca.* 650 nm when Pb^{2+} was added to the GSH–GNPs core–satellite solution, and the excitation was most effective when the excitation frequency was closed to the maxima of the plasmon band, 633 nm excitation laser was used for the SERS study in order to produce the optimal SERS results.

Raman spectrum was failed to obtain from aqueous GSH solution, thus Raman spectrum obtained from GSH powder was used as the reference (Fig. 2b). The SERS spectrum of GSH-functionalized GNPs (Fig. 2b) exhibited some strong features that corresponded very well with those of the spectrum of GSH powder. The disappearance of S–H peak at 2526 cm^{-1} (Fig. 2b), in particular, confirmed the hybridization of GNPs with GSH as Au-S bond was formed instead (Qian and Krimm, 1994). The peaks at 2865 to 2999 cm^{-1} found in the spectrum of GSH powder were assigned to be the symmetric and asymmetric stretching of C–H bonds, these peaks were surface-enhanced and formed a broaden peak at 2934 cm^{-1} when GNPs were functionalized with GSH. The two peaks enhanced greatly at 1475 and 1579 cm^{-1}, which were blue-shifted from the bands found in the reference spectrum at 1442 and 1450 cm^{-1}, were assigned to be the bending of C–H bonds. While the peak at 1359 cm^{-1}, which was blue-shifted from the peak at 1337 cm^{-1} of the spectrum of GSH powder was assigned to be the stretching of C–O bond.

The state of aggregation of nanoparticles plays an important role in the enhancement of SERS (Moskovits, 2005; Sztainbuch, 2006). After the addition of Pb^{2+}, the Raman spectroscopy was enhanced greatly (Fig. 2b), indicating the induction of the self-assembly of core–satellite structure by Pb^{2+}, which resulted in the formation of larger aggregates. Most of the peaks disappeared suggesting a lack of the previously existed zwitterion species (i.e. COO^- and C–NH_3^+). Pb^{2+} ions were bound to GSH and induced the self-assembly of core–satellite structure.

3.4. Kinetics

The formation of core–satellite structure caused changes in LSPR. UV–vis spectrum of different concentration of Pb^{2+} added to 1:1 (v/v) 13 nm to 45 nm GNPs with an overall GSH concentration of 100 μM at pH 5.5 were recorded. The kinetics were investigated to gain an insight into the process as we observed that the newly formed peak appeared faster when higher concentration of Pb^{2+} was added. Data from the UV–vis spectrum were used to plot the kinetics (Fig. S6). The kinetic curve for negative control was flat, and higher Pb^{2+} concentration increased the aggregation rate. The kinetic curves reached plateau after 30 min. Thus, to obtain a stable measurement, the incubation time for colorimetric detection was set at 30 min. The kinetic pattern was found to be very similar to the prior report (Weng et al., 2013).

3.5. Colorimetric detection of Pb^{2+}

To investigate the ability of the established core–satellite structure on Pb^{2+} detection, a calibration curve was obtained by recording the absorbance ratio when different concentrations of Pb^{2+} ions were added to the core–satellite samples. Each of the samples was incubated for 30 min before conducting UV–vis spectroscopy, and three independent measurements were carried out for each samples to provide statistical significance. The shifting in LSPR band is due to the coupled plasmon resonance of GNPs when the interparticle distance changes. The peaks at 650 nm and 525 nm were related to the quantity of aggregated and dispersed GNPs respectively. Thus A_{650}/A_{525} was used as the indicator in this study. A good linear relationship between A_{650}/A_{525} and concentration of Pb^{2+} was observed from 2 to 14 μM (R^2=0.9934) (Fig. 3a). The LOD was determined to be 47.6 nM (9.9 ppb) by 3σ rule, which was just lower than the WHO standard limit (10 ppb) (World Health Organization, 2008).

Several commonly existing heavy metals were used to test the selectivity of the assay. It was observed that 20 μM Ca^{2+}, Cd^{2+}, Co^{2+}, Cu^{2+}, Fe^{2+}, Mg^{2+}, Mn^{2+} and Ni^{2+} had no obvious effect on the color of 1:1 (v/v) 13 nm and 45 nm GSH–GNPs solution. While the solution changed from red to blue, due to the addition of 20 μM Pb^{2+}, indicating the system was highly selective toward Pb^{2+}. The changes in values of A_{650}/A_{525} upon the addition of 20 μM metal ions were also plotted (Fig. 3b), showing the high selectivity for Pb^{2+}. It is proposed that the configuration of core–satellite structure limited the species of ions to chelate with GSH, and the rate of aggregation induced by other metal ions was relatively slow compared to Pb^{2+}. However, further investigation is needed for the detailed mechanism of selectivity in the future work.

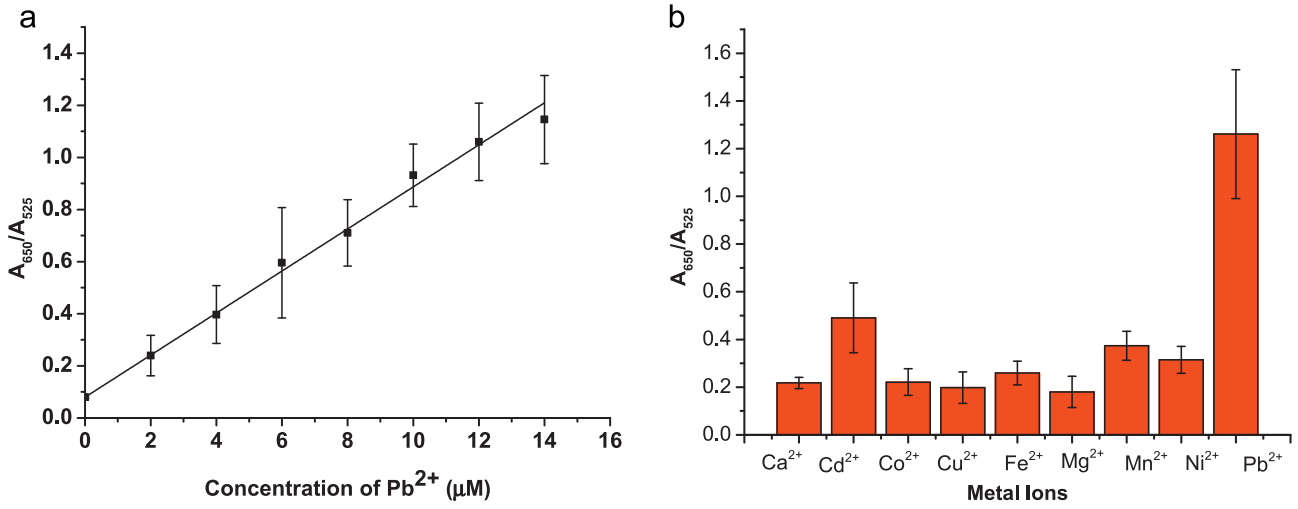

Fig. 3. (a) Fitted linear plot of A_{650}/A_{525} versus concentration of Pb^{2+}; (b) A_{650}/A_{525} upon the addition of 20 μM other metal ions. The error bars represent the standard deviations based on three independent measurements.

3.6. Analysis of real samples

In real-life application, the concentration of unknown contaminants in sample may be significantly greater than that of Pb^{2+}, thus causing interference with the test results, which is a critical problem to the application of many sensors developed. Untreated lake water collected from Deakin University Waurn Ponds Campus, Vic., Australia was spiked with known concentrations of Pb^{2+} to mimic the contamination of water to confirm the practical application of this assay. The detected Pb^{2+} concentration in lake water samples was shown in Table S1. The high recovery suggested that the core–satellite structure was not free from the matrix effect of the samples and may be selective towards other metal ions which were not tested in this study. Further investigation and modification were needed for the practical application of this method.

4. Conclusions

In this paper, we described a simple yet innovative colorimetric detection method for Pb^{2+} based on the self-assembly of GSH–GNPs core–satellite structures. The experimental results showed that the core–satellite structure can detect as low as 47.6 nM Pb^{2+} with high selectivity against other heavy metals. It is suggested such core–satellite structures through nature peptides could be utilized for development of highly sensitive and sensitive colorimetric detection methods for toxic heavy metals.

Acknowledgement

WY would like to thank Australian Research Council for the financial support (DPDP130101714).

Appendix A. Supplementary material

Supplementary data associated with this article can be found in the online version at http://dx.doi.org/10.1016/j.bios.2014.09.077.

References

Beqa, L., Singh, A.K., Khan, S.A., Senapati, D., Arumugam, S.R., Ray, P.C., 2011. ACS Appl. Mater. Interfaces 3 (3), 668–673.
Canesi, L., Viarengo, A., Leonzio, C., Filippelli, M., Gallo, G., 1999. Aquat. Toxicol. 46 (1), 67–76.
Chai, F., Wang, C., Wang, T., Li, L., Su, Z., 2010. ACS Appl. Mater. Interfaces 2 (5), 1466–1470.
Chen, J.I.L., Chen, Y., Ginger, D.S., 2010. J. Am. Chem. Soc. 132 (28), 9600–9601.
Cho, E.S., Kim, J., Tejerina, B., Hermans, T.M., Jiang, H., Nakanishi, H., Yu, M., Patashinski, A.Z., Glotzer, S.C., Stellacci, F., 2012. Nat. Mater. 11 (11), 978–985.
Choi, I., Song, H.D., Lee, S., Yang, Y.I., Kang, T., Yi, J., 2012. J. Am. Chem. Soc. 134 (29), 12083–12090.
Chou, L.Y., Zagorovsky, K., Chan, W.C., 2014. Nat. Nanotechnol..
Cutrignelli, A., Lopedota, A., Denora, N., Laquintana, V., Tongiani, S., Franco, M., 2014. J. Pharm. Sci. 103 (4), 1246–1254.
Encina, E.R., Coronado, E.A., 2010. J. Phys. Chem. C 114 (39), 16278–16284.
Fu, R., Li, J., Yang, W., 2012. J. Nanopart. Res. 14 (6), 1–8.
Guo, Z., Liu, Z.G., Yao, X.Z., Zhang, K.S., Chen, X., Liu, J.H., Huang, X.J., 2013. Sci. Rep., 3.
Huang, K.-W., Yu, C.-J., Tseng, W.-L., 2010. Biosens. Bioelectron. 25 (5), 984–989.
Jakubowski, M., 2011. Int. J. Occup. Med. Environ. Health 24 (1), 1–7.
Kalluri, J.R., Arbneshi, T., Afrin Khan, S., Neely, A., Candice, P., Varisli, B., Washington, M., McAfee, S., Robinson, B., Banerjee, S., 2009. Angew. Chem. 121 (51), 9848–9851.
Kim, S., Arora, M., Fernandez, C., Landero, J., Caruso, J., Chen, A., 2013. Environ. Res. 126 (0), 105–110.
Li, X., Wang, J., Sun, L., Wang, Z., 2010. Chem. Commun. 46 (6), 988–990.
Liu, J., 2011. Aggress. Violent Behav. 16 (1), 63–73.
Mao, X., Li, Z.-P., Tang, Z.-Y., 2011. Front. Mater. Sci. 5 (3), 322–328.
Moskovits, M., 2005. J. Raman Spectrosc. 36 (6-7), 485–496.
Pal, S., Sharma, J., Yan, H., Liu, Y., 2009. Chem. Commun. 40, 6059–6061.
Qian, W., Krimm, S., 1994. Biopolymers 34 (10), 1377–1394.
Schreiber, R., Do, J., Roller, E.-M., Zhang, T., Schüller, V.J., Nickels, P.C., Feldmann, J., Liedl, T., 2013. Nat. Nanotechnol..
Sebba, D.S., Lazarides, A.A., 2008. J. Phys. Chem. C 112 (47), 18331–18339.
Sebba, D.S., Mock, J.J., Smith, D.R., LaBean, T.H., Lazarides, A.A., 2008. Nano Lett. 8 (7), 1803–1808.
Stetzenbach, K.J., Amano, M., Kreamer, D.K., Hodge, V.F., 1994. Ground Water 32 (6), 976–985.
Sztainbuch, I.W., 2006. J. Chem. Phys 125 (12).
Weng, Z., Wang, H., Vongsvivut, J., Li, R., Glushenkov, A.M., He, J., Chen, Y., Barrow, C.J., Yang, W., 2013. Anal. Chim. Acta 803, 128–134.
Wilczek, G., Babczyńska, A., Augustyniak, M., Migula, P., 2004. Environ. Pollut. 132 (3), 453–461.
World Health Organisation, 2008. Guidelines for Drinking-Water Quality: Incorporating 1st and 2nd Addenda, vol.1, Recommendations, 3rd ed. World Health Organization, Geneva, Switzerland.
Yadav, S., 2010. S. Afr. J. Bot. 76 (2), 167–179.